SPACE WEATHER, VOL. 8, S05001, doi:10.1029/2009SW000488, 2010

Solar energetic particle cutoff variations during the 29–31 October 2003 geomagnetic storm

B. T. Kress,[1] C. J. Mertens,[2] and M. Wiltberger[3]

Received 24 April 2009; revised 21 January 2010; accepted 6 February 2010; published 13 May 2010.

[1] At low latitudes to midlatitudes the Earth's magnetic field usually shields the upper atmosphere and spacecraft in low Earth orbit from solar energetic particles (SEPs). During severe geomagnetic storms, distortion of the Earth's field suppresses geomagnetic shielding, allowing SEPs access to the midlatitudes. A case study of the 26–31 October 2003 solar-geomagnetic event is used to examine how a severe geomagnetic storm affects SEP access to the Earth. Geomagnetic cutoffs are numerically determined in model geomagnetic fields using code developed by the Center for Integrated Space Weather Modeling (CISM) at Dartmouth College. The CISM-Dartmouth geomagnetic cutoff model is being used in conjunction with the High Energy and Charge Transport code (HZETRN) at the NASA Langley Research Center to develop a real-time data-driven prediction of radiation exposure at commercial airline altitudes. In this work, cutoff rigidities are computed on global grids and along several high-latitude flight routes before and during the geomagnetic storm. It is found that significant variations in SEP access to the midlatitudes and high latitudes can occur on time scales of an hour or less in response to changes in the solar wind dynamic pressure and interplanetary magnetic field. The maximum suppression of the cutoff is ~1 GV occurring in the midlatitudes during the main phase of the storm. The cutoff is also significantly suppressed by the arrival of an interplanetary shock. The maximum suppression of the cutoff due to the shock is approximately one half of the maximum suppression during the main phase of the storm.

Citation: Kress, B. T., C. J. Mertens, and M. Wiltberger (2010), Solar energetic particle cutoff variations during the 29–31 October 2003 geomagnetic storm, *Space Weather*, *8*, S05001, doi:10.1029/2009SW000488.

1. Introduction

[2] Solar Energetic Particles (SEPs) are ions in the 10 to >500 MeV range produced by the Sun during solar active periods, usually in association with a solar flare or coronal mass ejection (CME). A solar particle event is a period of heightened SEP flux usually arriving at Earth tens of minutes after the associated solar event and lasting 1 to several days.

[3] SEPs are a space weather hazard posing risks to manned and robotic space flight missions. A solar particle event can expose astronauts, airline crews and passengers to increased levels of radiation [*Dyer et al.*, 2003]. Solar particle events are also damaging to electronic equipment in space and at high altitudes, causing degradation to micro electronics and single event upsets in micro electronics operations [*Tylka et al.*, 1996]. Large solar particle events have a global impact on the Earth's atmosphere. During a solar particle event >10 MeV protons penetrate below ~100 km altitude producing ionization that disrupts HF communication and navigation in the polar regions. The more energetic ions penetrate deep into the Earth's middle atmosphere to ~12–80 km causing changes in atmospheric constituents and dynamics [*Jackman et al.*, 2005; *Clilverd et al.*, 2005].

[4] Thermal solar wind ions with energies from one to several KeV have direct access to low Earth orbit and Earth's upper atmosphere only along interplanetary field lines, which have their foot points in the polar cap regions. More energetic ions however, with large gyroradii, can penetrate below the open/closed field line boundary to lower latitudes. The lowest latitude to which an energetic solar ion can penetrate is known as its *cutoff latitude* and is a function of the ion's momentum per unit charge, which is referred to as its rigidity. Equivalently, one may consider a *cutoff rigidity* corresponding to a given location within the geomagnetic field. The cutoff rigidity is the minimum rigidity particle with access to that location. Surfaces of constant cutoff rigidity in the magnetosphere approximately follow surfaces of constant L shell.

[1]Department of Physics and Astronomy, Dartmouth College, Hanover, New Hampshire, USA.
[2]NASA Langley Research Center, Hampton, Virginia, USA.
[3]High Altitude Observatory, National Center for Atmospheric Research, Boulder, Colorado, USA.

[5] During quiet geomagnetic periods the cutoff latitudes for most SEPs fall over a small range of latitudes near ~60° International Geomagnetic Reference Field (IGRF) invariant latitude, which corresponds to $L \sim 4$. During a geomagnetic storm the Earth's field is distorted modifying SEP access to the inner magnetosphere. During the main phase of the storm, the cutoff latitude can be suppressed up to ~15° equatorward, exposing normally shielded midlatitudes to radiation and increasing the polar cap area to which SEPs have access by a factor of 2–3 [*Labrador et al.*, 2003]. Using energetic particle measurements *Leske et al.* [2001] showed that geomagnetic cutoff variations during storms are correlated with the depression and recovery of the disturbance storm time (Dst) index, thus are primarily attributed to a reduction in field strength in the inner magnetosphere due to ring current buildup. Typically the cutoff (Rigidity and/or Latitude) is most suppressed during the main phase of the storm when the Dst reaches a minimum. *Leske et al.* [2001, p. 30,021] also note that "the correlation with Dst is worse at certain times, often during critical periods such as the onset of a geomagnetic storm when a large cutoff suppression can occur hours before the corresponding change in Dst." This finding is born out by results presented by *Kress et al.* [2004], who showed using observations and model results that an increase in the solar wind dynamic pressure (P_{dyn}) significantly suppresses the cutoff during the 24 November 2001 storm sudden commencement (SSC), hours before the main phase of the storm.

[6] The response of geomagnetic shielding to changes in solar wind conditions is not well understood. The increase in magnetic field strength in the inner magnetosphere associated with an SSC suggests that an enhancement in geomagnetic shielding would occur with an increase in P_{dyn}; for example, *Belov et al.* [2005] state that the cutoff rigidity increases at the beginning of a magnetic storm relative to its quiet time level due to the magnetopause current systems, but this is not always the case. *Lee and Kress* [2008] found that an increase in P_{dyn} may cause an increase or decrease in the cutoff, with an increase more likely near noon local time and a decrease more likely near midnight local time.

[7] To aid in understanding cutoff variations during storms, geomagnetic cutoffs can be numerically modeled by computing test particle trajectories in a geomagnetic field model. The standard approach to modeling geomagnetic cutoffs has been developed primarily by Smart and Shea [e.g., *Shea et al.*, 1965; *Smart et al.*, 2000; *Smart and Shea*, 1994, 2005]. Modeled geomagnetic cutoffs can also be used for space weather applications. Global grids of geomagnetic cutoff rigidities can be used to predict SEP and cosmic ray flux in the magnetosphere from an observed interplanetary spectrum [*Golightly and Weyland*, 1997; *Smart and Shea*, 2003; *Smart et al.*, 2006]. *Smart and Shea* [2003] and *Smart et al.* [2006] have computed world grids of vertical cutoff rigidities in the *Tsyganenko* [1989, hereafter T89] geomagnetic field model. The T89 model is parametrized by a single indicator of geomagnetic activity, the Kp index. By computing vertical cutoff rigidities in the T89 model at different values for the Kp index, *Smart and Shea* [2003] and *Smart et al.* [2006] have produced a look up table that can be used in conjunction with a near-Earth interplanetary solar proton flux spectrum to make a real time prediction of SEP flux in the Earth's magnetosphere.

[8] Several studies have been done to verify the accuracy of numerically modeled cutoffs. *Smart and Shea* [2001] compare cutoff latitudes computed in T89 with observations from the Solar Anomalous and Magnetospheric Particle Explorer (SAMPEX) spacecraft between 31 October and 7 November 1992. *Kahler and Ling* [2002] extended this work by comparing modeled and observed cutoff latitudes numerically determined in IGRF and T89 field models during nine SEP events. More recently, *Weygand and Raeder* [2005] computed cutoffs in the IGRF, T89, *Tsyganenko* [1996] and MHD magnetospheric field models during the 23–24 April 1998 geomagnetic storm. The numerically modeled cutoff latitudes determined in these studies typically agree with observations to within a few degrees; for example, *Kahler and Ling* [2002] find that on average the modeled cutoff latitudes differ from observed by $\Delta\lambda = 2°$. *Kahler and Ling* [2002] also find that the observed cutoff latitudes are systematically equatorward of the modeled cutoff latitudes.

[9] In the work presented here, a case study of the 26–31 October 2003 solar-geomagnetic event is used to examine how a severe geomagnetic storm globally affects SEP access to the Earth. Cutoff rigidities are computed using the CISM-Dartmouth geomagnetic cutoff code, which may be run using several different empirical and physics based geomagnetic field models. For this work, cutoff rigidities are computed in empirical model fields of *Tsyganenko and Sitnov* [2005, hereafter TS05], and also in fields from the Lyon-Feder-Mobarry (LFM) global MHD magnetospheric simulation code [*Lyon et al.*, 2004]. The CISM-Dartmouth cutoff code is being used in conjunction with the High Energy and Charge Transport code (HZETRN) at NASA Langley Research Center to aid in the development of the Nowcast of Atmospheric Ionizing Radiation for Aviation Safety (NAIRAS) model. The goal of the NAIRAS project is to develop a prototype real-time data-driven prediction of atmospheric radiation. The cutoff rigidity code provides a dynamic outer boundary condition for the HZETRN atmospheric transport code. Cutoff rigidities computed along several polar flight routes during the 26–31 October 2003 solar-geomagnetic event are presented in section 3.4 of this paper. The corresponding dose rates and accumulated dose obtained from the HZETRN transport code are presented in a companion paper [*Mertens et al.*, 2010]. It is found that the difference in total SEP dose at commercial aircraft altitudes determined using cutoff rigidities computed in the Earth's internal field only (i.e., the static IGRF field model), versus using cutoffs computed in dynamic TS05 model fields, underestimates the total SEP dose at commercial aircraft altitudes by approximately 40% to over a factor of 3. The total difference in dose when the effect of both the SEPs and galactic cosmic rays are

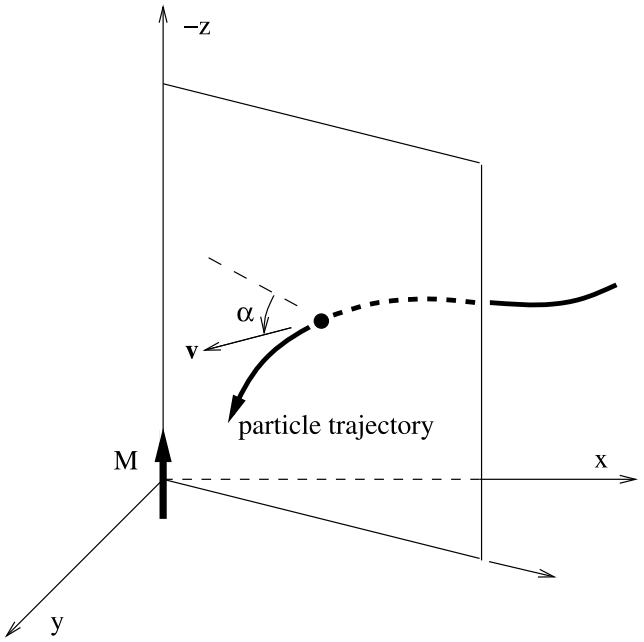

Figure 1. Particle trajectory in a dipole magnetic field. Here α is the angle between the particle velocity and the meridional plane intersecting the particle position. When α = 90° the particle is traveling in the magnetic east direction, and when α = –90° the particle is traveling toward magnetic west.

included will be somewhat less however, since the galactic cosmic ray intensity is reduced during solar active periods.

[10] An outline of the paper is as follows. In section 2 a review of how geomagnetic shielding is quantified in terms of cutoff rigidity is given. A number of important definitions are in section 2 including definitions of the cutoff latitude, cutoff rigidity, vertical cutoff rigidity, and upper and lower vertical cutoff rigidities. Section 3 gives a brief description of the numerical techniques used to compute cutoffs for this work. This is followed by comparisons between numerically determined cutoffs and observations, including a detailed description of how the cutoff rigidities are extracted from SAMPEX data. The comparison between the modeled and observed cutoff latitudes show that the model follows storm time variations in the cutoff reasonably well. Global maps of cutoff rigidities at selected times during 26–31 October 2003 and cutoff rigidities computed along three polar flight routes are also included in section 3. The corresponding dose rates and accumulated dose for the flights are presented in the companion paper by *Mertens et al.* [2010]. A summary and discussion of results is presented in section 4.

2. Theory/Background

2.1. Cutoff Rigidity and Cutoff Latitude

[11] The lowest latitude to which an energetic solar ion of given rigidity can penetrate is known as its *cutoff latitude* and is a function of the strength of the dipole moment and the ion's rigidity. Alternatively one may consider a *cutoff rigidity* corresponding to a given location in space in the vicinity of a dipole field. Particles with rigidities below the cutoff rigidity do not have access to that location. *Störmer* [1955] first obtained an analytical expression for the cutoff latitude/rigidity of a charged particle incident on a pure dipole magnetic field. In this section Störmer's result is presented along with a brief discussion of how it applies to geomagnetic shielding. The *vertical cutoff rigidity* is also defined together with a description of how shadowing of energetic particle trajectories by the solid body of the Earth leads to the definition of upper and lower vertical cutoff rigidities.

[12] Consider a charged particle incident on a pure dipole magnetic field with the dipole moment oriented along the z axis. Using conservation of the particle's kinetic energy and the azimuthal component of its generalized momentum, *Störmer* [1955] showed that the particle is classically forbidden, by a magnetic potential barrier, from entering a toroidal region surrounding the dipole. The boundary of this region is defined by the equation

$$r = \sqrt{\frac{M}{R}} \frac{\cos^2 \lambda}{1 + \sqrt{(1 + k\cos^3 \lambda)}}, \tag{1}$$

where r is the radial distance from the center of the dipole, λ is the latitude, M is the dipole moment, R is the rigidity, and k is the sine of the angle α between the particle velocity and the meridional plane that intersects the particle position (see Figure 1). When k = +1 the particle is traveling in the magnetic east direction and when k = –1 the particle is traveling toward magnetic west. Note that the smallest obtainable value of r occurs when k = +1; that is, the point of closest approach to the center of the dipole occurs when the particle is traveling directly toward magnetic east.

[13] The surface of rotation of the curve defined by equation (1) about the z axis is the boundary enclosing *Störmer*'s [1955] forbidden region. Particles incident from outside the influence of the dipole magnetic field do not have access inside of this boundary. As an example, Figure 2 shows the cross section of the forbidden region for a 200 MeV proton (R = 0.64 GV) incident on a magnetic dipole with $M = 8.05 \times 10^{25}$ gauss-cm^3, which is an appropriate value for a dipole used as a simple model of the Earth's magnetic field. The intersection of Störmer's boundary with the Earth's surface at approximately 60° latitude corresponds to the location of the cutoff latitude. At higher rigidities the size of the forbidden region becomes smaller and the cutoff latitude moves toward the equator.

[14] Alternatively, if equation (1) is solved for the rigidity,

$$R_C = C_{St} \frac{\cos^4 \lambda}{r^2} \frac{1}{\left(1 + \sqrt{(1 + k\cos^3 \lambda)}\right)^2}, \tag{2}$$

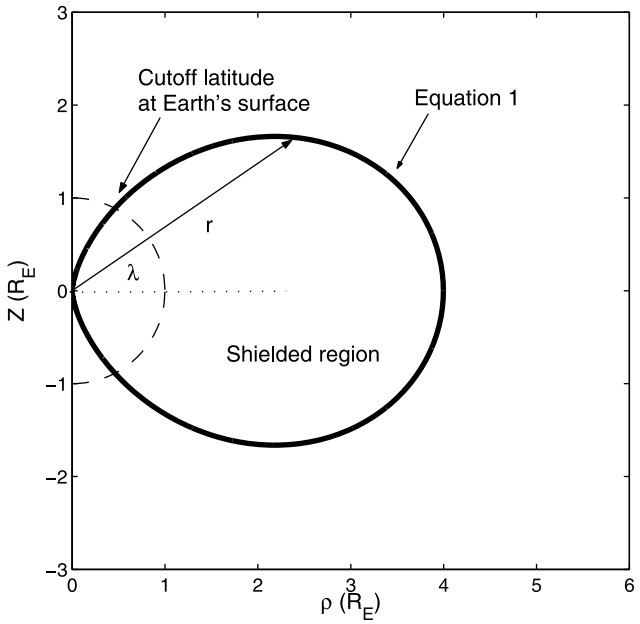

Figure 2. Boundary of *Störmer*'s [1955] forbidden region for a 200 MeV proton incident on a magnetic dipole model of the Earth's field. Distances are given in units of Earth radii (R_E).

we obtain the *cutoff rigidity* R_C as a function of location. The constant $C_{St} \approx 60$ contains the dipole moment and the conversion factors needed to express the rigidity in units of GV when r is in units of Earth radii. The cutoff rigidity R_C is the lowest rigidity particle, incident from outside the influence of the magnetic field, that has access to a given location in space. Surfaces of constant R_C in a dipole model of the Earth's magnetic field are a set of surfaces like the one shown in Figure 2 parametrized by rigidity and direction of arrival. Their intersections with a spherical surface at 1 R_E are rings of constant latitude, with cutoff rigidities beginning at zero at the magnetic pole and increasing up to approximately 60 GV at the magnetic equator (corresponding to a 59 GeV proton arriving from magnetic east). At rigidities $\gtrsim$60 GV the cutoff surfaces lie completely inside of the Earth, thus there is no magnetic shielding by the Earth of particles with rigidities greater than ~60 GV.

2.2. Vertical Cutoff Rigidity

[15] An estimate of the SEP flux at a location in the magnetosphere can be obtained from the cutoff rigidity as follows. If one assumes an isotropic particle flux in interplanetary space, Liouville's theorem requires that at rigidities above the cutoff rigidity the directional flux of particles in the magnetosphere is equivalent to that outside the influence of the geomagnetic field [*Lemaitre and Vallarta*, 1933; *Swann*, 1933]; that is, the flux of particles with rigidities above the cutoff rigidity is the same as in interplanetary space, and the flux of particles with rigidities below the cutoff rigidity is zero. Thus, the energetic particle flux at a given location in the magnetosphere is obtained by integrating over the interplanetary particle spectrum at rigidities exceeding the cutoff rigidity at that location.

[16] The approach described above is complicated by the addition of the solid body of the Earth which intercepts a portion of the SEP trajectories. In the Earth's upper atmosphere and in low Earth orbit ~2π steradians are blocked by the Earth, and the flux is reduced by approximately one half. In space, since the cutoff rigidity is lowest for particles arriving from the west, the maximum SEP flux is from the west. As we descend into the Earth's upper atmosphere, however, the direction of arrival of the maximum SEP flux approaches the zenith. This is because SEPs arriving from the vertical direction traverse the least atmospheric mass and are thus least attenuated by collisions with atmospheric constituents. In early studies involving atmospheric measurements this led to the use of the vertical cutoff rigidity R_{CV} [*Smart and Shea*, 1994]. If only particles from the zenith direction are considered, we set $k = 0$ in equation (2) to obtain

$$R_{CV} = \frac{C_{St}}{4L^2}, \tag{3}$$

where $L = r/\cos^2\lambda$ is the dipole L shell. Use of R_{CV} has the advantage of removing λ from the denominator of equation (2) and allowing us to combine r and the remaining λ so that the cutoff is expressed in terms of L alone. The *vertical cutoff rigidity* is the lowest rigidity particle arriving from the zenith direction that has access to a given location within the field.

[17] Additional complication is introduced by the inclusion of the solid body of the Earth. Since particle trajectories are bent due to the influence of the magnetic field, some particle trajectories arriving from directions above the Earth's horizon are also blocked by the Earth, including some trajectories arriving from the zenith direction. The result is a shadow or *penumbral* region containing bands of forbidden and allowed trajectories at rigidities above the magnetic cutoff rigidity. In order to characterize the penumbral region, one may define a *lower vertical cutoff rigidity* R_L below which all particle trajectories are shielded, either by the solid body of the Earth or due to magnetic shielding; and an *upper vertical cutoff rigidity* R_U above which no particle trajectories are shielded. In practice, to account for the penumbral region, an effective cutoff rigidity between R_L and R_U may be used for space weather applications [*Shea et al.*, 1965].

3. Numerical Results

3.1. Overview of Numerical Techniques for Computing Cutoffs

[18] In a pure dipole, the cutoff rigidity is an analytically expressible function of the dipole strength and the location in the field. In an arbitrary geomagnetic field model

however, it is necessary to determine cutoffs numerically. The standard technique is to launch time reversed Lorentz particle trajectories from a point in space to determine particle access to that location [*Smart et al.*, 2000]. Particles of different rigidity are launched and each trajectory is followed backward in time. If a particle escapes the magnetosphere then a viable inward trajectory has been found indicating that the particle's rigidity is above the cutoff rigidity. The CISM-Dartmouth geomagnetic cutoff code uses a numerical search algorithm following *Orloff* [1999]. The penumbral region is first located using a bisection method [e.g., *Press et al.*, 1992]. Then the lower vertical cutoff rigidity R_L is located by taking small steps upward in rigidity from below the penumbra until a single particle escapes. The rigidity step size for the sequential search is ~1% of the total rigidity. All computed cutoffs presented in this paper are lower vertical cutoff rigidities R_L. For the remainder of the paper, "cutoff rigidity" or simply "cutoff" is used to refer to R_L.

[19] Lorentz trajectories are computed using a fourth-order Runge-Kutta integrator. The time step is continuously adapted to be approximately one one hundredth of the particle gyroperiod. Fast integration is achieved by linearly interpolating magnetic fields from a Cartesian grid to the particle position. Trajectories are computed in static magnetic field model snapshots ignoring the electric field and interaction with magnetospheric oscillations. This is appropriate for SEPs that typically interact with the magnetosphere on time scales short compared to magnetospheric dynamics. A rare exception is during an SSC when globally coherent magnetospheric electric fields ~0.1 V/m can be produced by the impact of a high-speed interplanetary shock on the magnetosphere. Occasionally during these events SEPs are transported inward in L and energized by the SSC pulse forming new belts of energetic ions at low L. Flux enhancements caused by these new belts are not included in a model of SEP flux based solely on geomagnetic cutoffs. These enhancements however are typically 1 to several orders of magnitude less than the SEP flux in regions above the SEP cutoff. For example, see Figure 1 of *Kress et al.* [2004] which shows that the newly trapped >25 MeV proton belt appearing at $L \sim 3$ following the 23–24 November 2001 SEP event is 1–2 orders of magnitude less intense than the >25 MeV flux level at $L \gtrsim 3$ during the SEP event.

[20] A difficulty arises when calculating the cutoff rigidity near the open/closed field line boundary. Since all particles have access to the polar cap region, as the open/closed boundary is approached from the equatorward direction the cutoff rigidity approaches zero. Since the integration time step is proportional to the gyroperiod, as the cutoff rigidity approaches zero the integration step size also approaches zero. Thus, as the open/closed boundary is approached, very long times are needed to integrate a particle trajectory with the minimum rigidity needed to escape the magnetosphere. This difficulty is avoided by setting a minimum rigidity R_{min} in the code. At locations poleward of the R_{min} cutoff rigidity contour the cutoff rigidity is obtained by interpolating between R_{min} at the position of the R_{min} contour and zero at the open/closed boundary, located using a field line tracing algorithm. In the work presented here R_{min} = 0.05 GV corresponding to an ≈1 MeV proton.

[21] The CISM-Dartmouth geomagnetic cutoff code can be run using several different empirical and physics-based geomagnetic field models. In this work, cutoff rigidities are computed in empirical model fields of *Tsyganenko and Sitnov* [2005], and also in fields from the Lyon-Feder-Mobarry (LFM) global MHD magnetospheric simulation code [*Lyon et al.*, 2004]. Solar wind input parameters for the TS05 and LFM models during 26–31 October 2003 were obtained from the ACE and Geotail spacecraft. Information about acquisition and processing of the 26–31 October 2003 solar wind data is available in the work by *Lopez et al.* [2007]. The LFM MHD code may be run as a stand alone model or coupled with other geospace models currently in use within CISM, e.g., the Rice Convection Model (RCM) [*Toffoletto et al.*, 2004], which models the ring current using an adiabatic drift formalism, and/or the Thermosphere-Ionosphere Nested Grid (TING) model [*Wang et al.*, 2004]. We have found that the TS05 empirical model provides more accurate cutoff rigidities than the stand alone LFM MHD model. Geomagnetic cutoffs determined in LFM fields during storms are usually too high. This is mainly due to the lack of a full kinetic description of the ring current in the MHD model. However, the fully coupled LFM-TING-RCM model currently under development within CISM is expected to provide a physics based geomagnetic field model that will include short time scale dynamics not included in empirical models.

3.2. Comparison With SAMPEX Observations

[22] The Solar Anomalous and Magnetospheric Particle Explorer (SAMPEX) spacecraft is in a low Earth polar orbit at approximately 600 km altitude and has a 90 min orbital period [*Baker et al.*, 1993]. Its 8° inclination with respect to the geographic pole brings it above approximately 66° (or below −66°) IGRF invariant magnetic latitude with each pass over the north (or south) polar region. The energetic particle data used for comparison with the model results is 30 s averaged proton flux measured by the proton electron telescope (PET) instrument on board SAMPEX. The SAMPEX/PET data is provided by Glenn Mason (JHU/APL) via the Coordinated Data Analysis Web site.

[23] Figure 3 (top) shows PET 19–27 MeV proton flux during 28–31 October 2003. The SEP event begins on the latter half of 26 October 2003 at ~1800 UT [*Mewaldt et al.*, 2005]. The significantly elevated SEP flux shown in Figure 3 begins on 28 October 2003 continues until 31 October 2003. The discontinuous appearance of the flux in Figure 3 is due to SAMPEX's 90 min orbital period. Each spike corresponds to a pass over the north or south polar cap. When the spacecraft is equatorward of the cutoff latitude the observed proton flux falls to near zero.

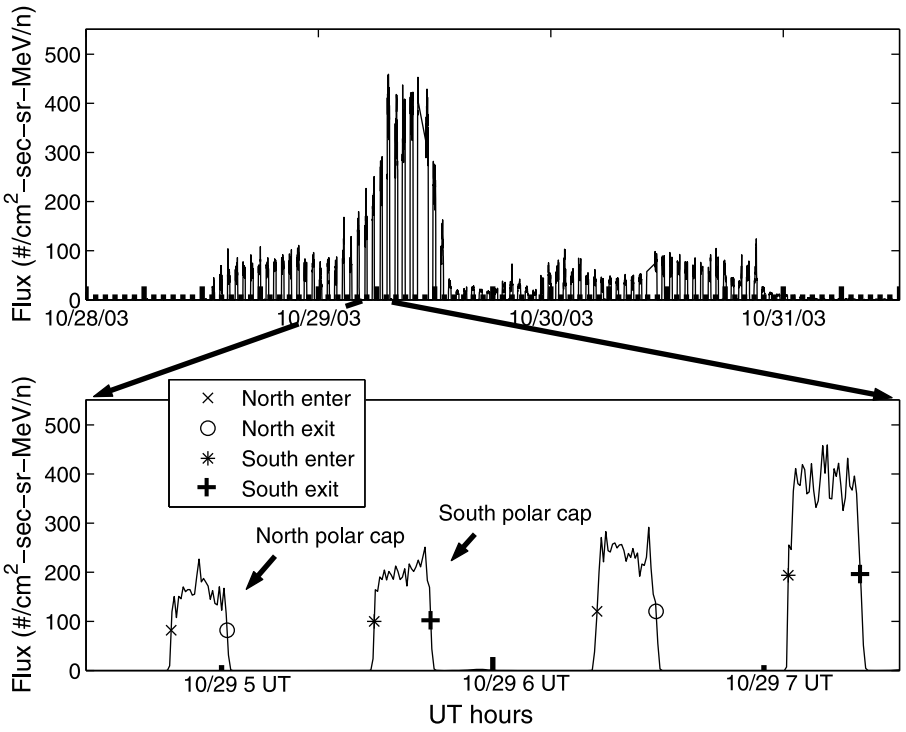

Figure 3. SAMPEX/PET 19–27 MeV proton flux during the October–November 2003 solar-geomagnetic event. (top) The period from 28 to 31 October. (bottom) Several hours on 29 October during which SAMPEX made four passes over the north and south polar cap regions. The cross, circle, star, and plus symbols indicate the times when SAMPEX passes the north enter, north exit, south enter, and south exit cutoffs, respectively.

[24] A numerical algorithm has been developed to extract cutoff latitudes from the SAMPEX data using a technique similar to one used by *Leske et al.* [2001]. Figure 3 (bottom) illustrates where cutoff latitudes are determined in the data. The algorithm first reads through the SAMPEX/PET flux data file, identifies polar cap passes and calculates the average polar cap flux for each pass. The average polar cap flux is taken to be the mean flux above 65° IGRF invariant magnetic latitude. The routine then searches for transitions from below to above or above to below one half the polar cap average. The cutoff latitude is taken to be the latitude where the flux exceeds or falls below one half of its average polar cap value. The two most equatorward such transitions are selected as the entering and exiting cutoff latitudes. Care is taken to ignore flux variations in the South Atlantic Anomaly region where particles trapped in the energetic ion belts have access to SAMPEX altitude. Four cutoff latitudes are obtained from each SAMPEX orbit as the spacecraft enters and exits the north and south polar cap regions. Four different symbols (cross, circle, star and plus) have been used in Figure 3 to denote the time and flux level where the spacecraft passes the cutoff in each case. The IGRF invariant magnetic latitude at the location of the cutoff is obtained from the SAMPEX data file using a linear interpolation between the 30 s data records (i.e., to the point where the linearly interpolated flux level exceeds or falls below half of its mean polar cap value.) The cutoff latitudes obtained from the 26–31 October 2003 event are plotted as a function of time in the first panel of Figure 4. During quiet magnetospheric conditions the SEP cutoff is at $L \sim 4$ corresponding to ~60° magnetic latitude. Deviation of the cutoff from ~60° is due to the inadequacy of the IGRF field model during the geomagnetic storm, which has been used for mapping the spacecraft position to a magnetic latitude. P_{dyn}, IMF B_Z and Dst index are also shown in Figure 4 for comparison. A large interplanetary shock shown by the dramatic increase in P_{dyn} arrives at the Earth's magnetosphere at ~0600 UT on 29 October 2003. The initial suppression of the cutoff is coincident with the arrival of the shock. Additional suppression of the cutoff is subsequently caused by weakening of the magnetic field in the inner magnetosphere due to ring current buildup, indicated by the decreasing Dst index. Suppression of the cutoff during the main phase of the storm, on the later half of 29 October 2003, is also caused by a strong southward IMF B_Z.

[25] Occasionally the numerical algorithm for extracting cutoff latitudes from the SAMPEX data returns no cutoff latitude or a bad value for the cutoff latitude. During 26–31 October 2003, the two main reasons for a missing or poor cutoff latitude are as follows. First, if either PET flux value

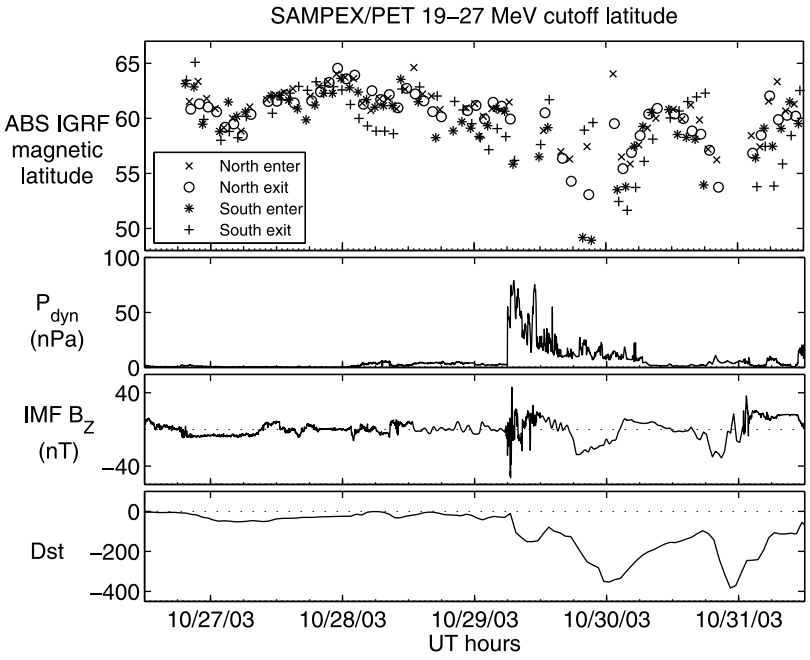

Figure 4. Observed cutoff latitudes versus time during the 26–31 October 2003 event (first panel). Also shown are the solar wind dynamic pressure and IMF B_Z from Geotail and ACE and the *Dst* index from the Kyoto Dst index service.

bounding one half the polar cap average is missing or flagged bad then no cutoff latitude is returned by the routine. Second, the cutoff latitude is sometimes poorly defined due to rapid time variations in the interplanetary SEP flux and/or structure in the polar cap region. In this case the cutoff latitude returned by the algorithm is shifted poleward. An example of this is illustrated in Figure 5, which shows the SAMPEX/PET 19–27 MeV proton flux during a single polar cap pass. Note that the cutoff determination is poleward of where the flux rises significantly above zero, due to large temporal and/or spatial variations in the polar region not associated with the cutoff.

[26] The modeled cutoff latitudes for comparison with SAMPEX observations are obtained as follows. Cutoff rigidities are determined (as described earlier in this section) by computing energetic particle trajectories in TS05 model geomagnetic fields. The cutoff rigidities are determined at a series of points along SAMPEX's trajectory, each point separated by ~2° latitude corresponding to the 30 s intervals between the records in the SAMPEX data file. A linear interpolation between these rigidities is used to find the location where the rigidity is equivalent to the midpoint of the 19–27 MeV proton PET detector energy channel; that is, 23 MeV which is equivalent to 0.21 GV for protons. The IGRF invariant magnetic latitude at this location, also obtained by a linear interpolation from the SAMPEX data file, is taken as the modeled cutoff latitude.

[27] The comparison between modeled and observed cutoff latitudes is shown in Figure 6. The four cases, north enter, north exit, south enter, and south exit are shown separately. The modeled cutoff latitudes are connected by a solid line in Figure 6, while the observed cutoff latitudes are shown as a series of markers. There are a total of

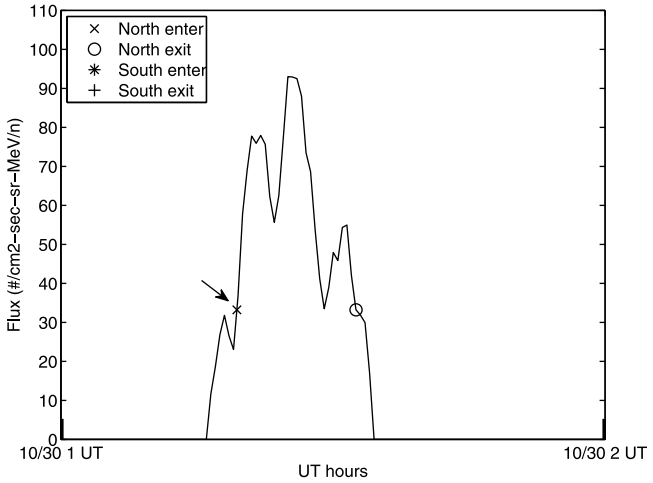

Figure 5. An example of SAMPEX/PET 19–27 MeV proton flux during a single pass over the north polar cap region that shows how significant flux variations in the polar cap region result in a cutoff latitude determination that is shifted poleward. The corresponding cutoff latitude is shown by an arrow in Figure 6 (top left).

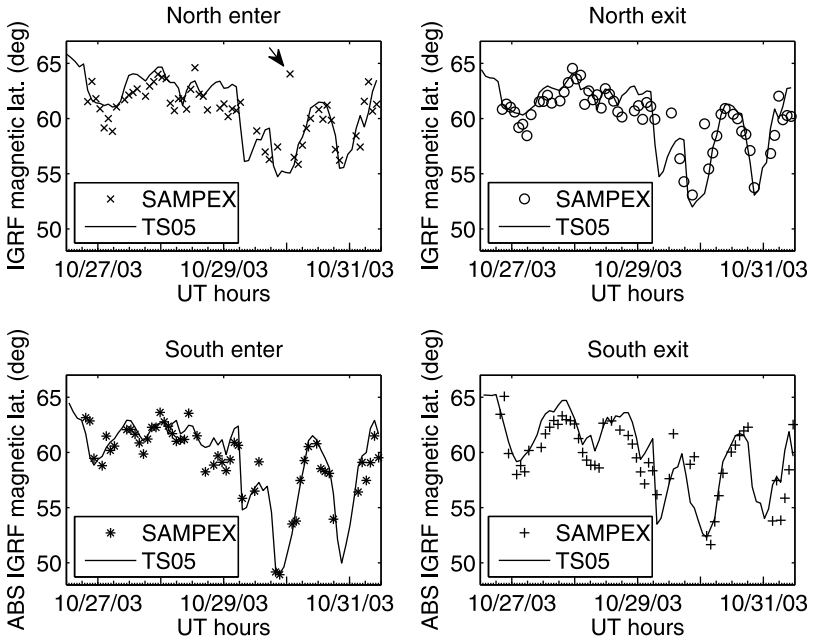

Figure 6. Comparisons between cutoff latitudes determined in the TS05 geomagnetic field model and cutoff latitudes extracted from SAMPEX PET energetic particle data during the 26–31 October 2003 solar-geomagnetic event.

298 modeled cutoff latitudes included in the four panels. During the same time interval 218 observed cutoffs were obtained from the SAMPEX/PET flux measurements, somewhat less than the number of modeled cutoffs primarily due to bad data flags (i.e., if the position of the spacecraft is known but the PET flux data is flagged bad then a modeled cutoff can be obtained while an observed cutoff cannot). To estimate the uncertainty associated with the cutoff latitude determination, the observed cutoff latitudes are compared with their corresponding modeled cutoff latitudes. Using the 218 cases where both modeled and observed values are available, the root mean square deviation of the difference between the modeled and observed cutoff latitudes is $\Delta\lambda_C = 1.8°$ magnetic latitude. The mean difference between the absolute values of the modeled and observed cutoff latitudes (modeled minus observed) is 0.60° indicating that on average the modeled cutoff latitudes are systematically 0.60° poleward of the observed cutoff latitudes.

[28] In a number of cases, the observed cutoff is not well defined due to large spatial or temporal variations of the SEP flux in the polar cap region as shown in Figure 5. The cutoff latitude indicated by the arrow in Figure 6 (top left) corresponds to the cutoff determination indicated by the arrow in Figure 5. There are several observed cutoff latitudes appearing in Figure 6 that are too high due to the lack of a distinct transition from zero to the polar cap average flux. If modeled and observed cutoff latitudes separated by more than 2 standard deviations are not included in the error calculation (the 5 most separated modeled and observed cutoff latitudes in Figure 6), then the root mean square deviation obtained is $\Delta\lambda_C = 1.5°$.

3.3. Globally Mapped Cutoffs in TS05 Model Fields

[29] Global maps of cutoff rigidities computed on a 5° × 5° latitude-longitude grid at ~600 km altitude in TS05 fields are shown in Figure 7. Figure 7 (top) is a contour plot of the prestorm cutoffs at 0200 UT on 28 October 2003 when Dst = –24 nT. Figure 7 (bottom) shows cutoffs during the main phase of the storm at 2100 UT on 29 October 2003 when Dst = –253 nT. Three great circle flight routes shown by the thick dashed lines are discussed in section 3.4. Before the start of the geomagnetic storm the northern portion of the continental US lies between the 1 GV and 2 GV contours, while during the main phase of the storm the same region is between the 0.1 GV and 1 GV contours. The proton energies corresponding to rigidities 0.1, 1 and 2 GV are ~5, 430 and 1300 MeV, respectively.

[30] The difference between cutoff rigidities before and during the storm are shown in Figure 8. The difference between the prestorm and shock arrival cutoff rigidities is shown in Figure 8 (top), and the difference between the prestorm and main phase cutoff rigidities is shown in Figure 8 (bottom). In each case storm time minus prestorm cutoffs are shown. The maximum suppression of ~1.1 GV occurs during the main phase of the storm at ~2100 UT on 29 October 2003 in the midlatitudes on the duskside of the Earth (Figure 8, bottom). The cutoff is also significantly lowered by the arrival of the interplanetary shock at 0611 UT on 29 October 2003 (Figure 8, top). The shock has the largest effect in the midlatitudes on the nightside. The

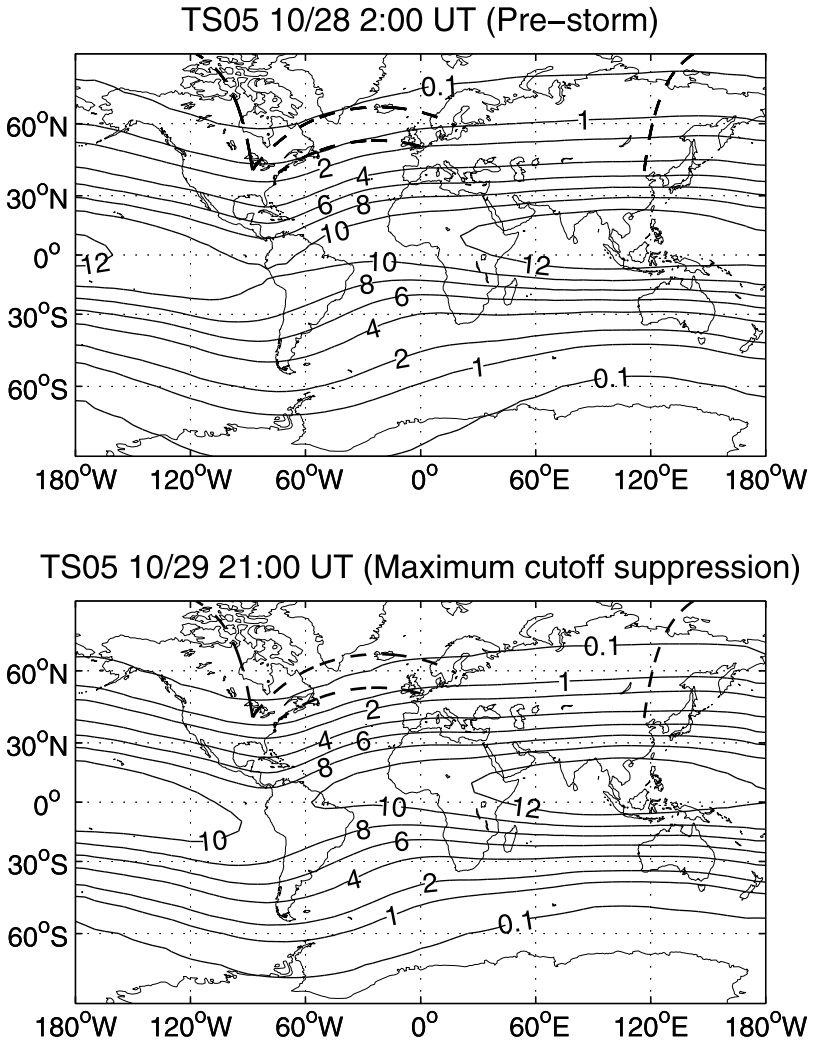

Figure 7. Cutoff rigidity maps computed on a 5° × 5° latitude-longitude grid at ~600 km altitude in TS05 model geomagnetic fields. (top) Prestorm cutoff rigidities at 0200 UT on 28 October 2003 and (bottom) when the maximum suppression of the cutoff occurs at 2100 UT on 29 October 2003. The thick dashed lines are three great circle flight routes from London to New York, Chicago to Stockholm, and Chicago to Beijing.

maximum suppression of the cutoff produced with the arrival of the interplanetary shock is ~0.5 GV, about one half of the maximum suppression during the main phase of the storm.

[31] Cutoff rigidity maps like the ones shown in Figure 7 were computed at 1 h intervals over the period 28–31 October 2003. The maximum suppression of the cutoff of ~1.1 GV was found to occur during the main phase of the storm at ~2100 UT on 29 October 2003 when Dst = −253 nT. Following this, the Dst continues to lower until it reaches a minimum of −353 nT at 0100 UT on 30 October 2003. Since ring current buildup is expected to be the primary cause of cutoff suppression, it is surprising that additional suppression of the cutoff does not occur as the Dst approaches a minimum. The largest cutoff suppression in the 0100 UT 30 October 2003 global map, when the Dst is at a minimum, is ~0.9 GV (not shown), also occurring in the mid-latitudes on the duskside. Comparison of the TS05 input parameters at the time of the maximum cutoff suppression with those at minimum Dst reveals that the greater cutoff suppression at 2100 UT on 29 October is due to a significantly enhanced partial ring current. During the maximum cutoff suppression the TS05 input parameter controlling the partial ring current is larger than it is at 0100 UT on 30 October, while at 0100 UT on 30 October the TS05 input parameter controlling the symmetric ring current is larger and the parameter controlling the partial ring current is smaller. The more enhanced partial ring current at ~2100 UT on 29 October is due to a strongly southward IMF B_Z ~ −20 nT. Careful inspection of

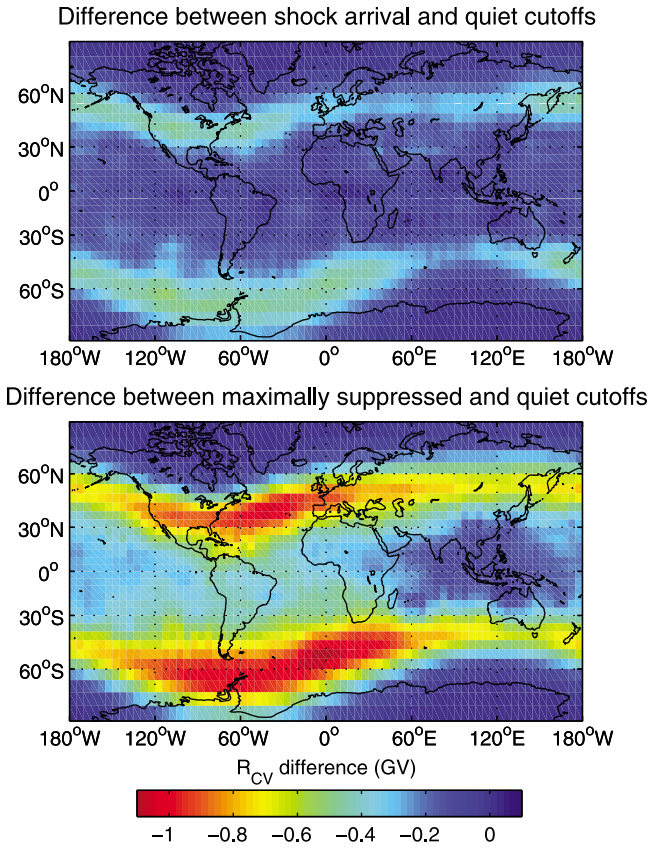

Figure 8. (top) Difference between prestorm cutoff rigidities and cutoffs at 0612 UT 29 October 2003, approximately 1 min after the arrival of the shock at the magnetosphere. Red shows the regions of greatest suppression of the cutoff. Noon local time at 0612 UT, 29 October 2003 is at approximately 90°E, indicating that the maximum suppression of the cutoff with the shock arrival is on the nightside. (bottom) Difference between prestorm cutoff rigidities and cutoffs when the maximum suppression of the cutoff occurs during the main phase of the storm at 2100 UT, 29 October 2003. Noon local time at 2100 UT, 29 October 2003 is at approximately 130°W, showing that the maximum suppression occurs in the dusk sector.

Figures 4 and 6 confirm that the recovery of the cutoff after 2100 UT on 29 October 2003 occurs in conjunction with a *decreasing* Dst and *increasing* IMF B_Z.

[32] The maximum suppression of the cutoff at ~2100 UT on 29 October 2003 can also be seen in the observed and modeled cutoff latitudes shown in the north exit and south enter panels of Figure 6. SAMPEX's precession with respect to a local time coordinate system has an ~80 day period. Since geomagnetic storms typically persist for 2–3 days SAMPEX remains approximately in the same local time meridional plane over the course of a storm. During 26–31 October 2003 SAMPEX's polar orbit was near the dawn-dusk meridional plane, with the northward portion of its orbit near 6 h local time and the southward portion of its orbit near 18 h local time. The maximum suppression of the cutoff at ~2100 UT on 29 October 2003 appearing in the north exit and south enter panels of Figure 6 corresponds to the southward portion of SAMPEX's orbit on the duskside where the maximum suppression also appears in Figure 8.

3.4. Cutoffs Along Aircraft Flight Routes

[33] In 1912 Austrian physicist Victor Francis Hess discovered an increase in the flux of cosmic radiation as he ascended in a balloon to ~16,000 ft. It is now known that the dose rate from cosmic radiation at typical commercial aircraft altitudes of ~35,000–40,000 feet is 2–3 orders of magnitude higher than at sea level. As a result, airline flight crews are typically exposed to more harmful radiation than nuclear plant workers. This led the European Union's Joint Aviation Authority in 2001 to enact a regulation that requires European airlines to monitor in-flight radiation exposure by airline crews. The European airlines must reduce the flying time of highly exposed crew members and reassign pregnant women to nonflying duties [*Bartlett*, 2004].

[34] To address the need for understanding and monitoring radiation dose along high-altitude flights, the CISM-Dartmouth cutoff code is being used in conjunction with the High Energy and Charge Transport code (HZETRN) at NASA Langley Research Center to develop a prototype real-time data-driven prediction of atmospheric radiation. The cutoff rigidity code provides a dynamic outer boundary condition for the HZETRN atmospheric transport code. As a test case, cutoff rigidities were computed along several polar flight routes using model fields from the 26–31 October 2003 solar-geomagnetic event. Three of the polar flight routes used for the study are shown by the thick dashed lines in Figure 7: from London to New York, Chicago to Stockholm and Chicago to Beijing. Cutoff rigidities computed along these flight routes in the IGRF, TS05 and LFM MHD field models are shown in Figure 9. The TS05 (blue and red curves) and LFM MHD (cyan and magenta curves) cutoffs were computed during a prestorm quiet period and during the main phase of the storm. The prestorm flights were all initiated at 0200 UT on 28 October 2003 and the storm time flights were initiated at 2100 UT on 29 October 2003. The cutoffs in each case are computed at 300–600 locations at 100 km altitude directly above the flight path, which is the outer boundary of the HZETRN transport code.

[35] The maximum suppression of the geomagnetic cutoff during the storm is ~1 GV occurring in the midlatitudes. Since most SEPs are <500 MeV the change in cutoff has the greatest effect on SEP exposure poleward of the 1 GV contours shown in Figure 7 (A 500 MeV proton has a rigidity of ~1.1 GV.). The result is that the greatest difference between prestorm and storm time exposure to SEPs occurs when a significant portion of the flight remains near but below the open/closed field line boundary. The London to New York and Chicago to Stockholm flights are cases where virtually all SEPs are shielded from the

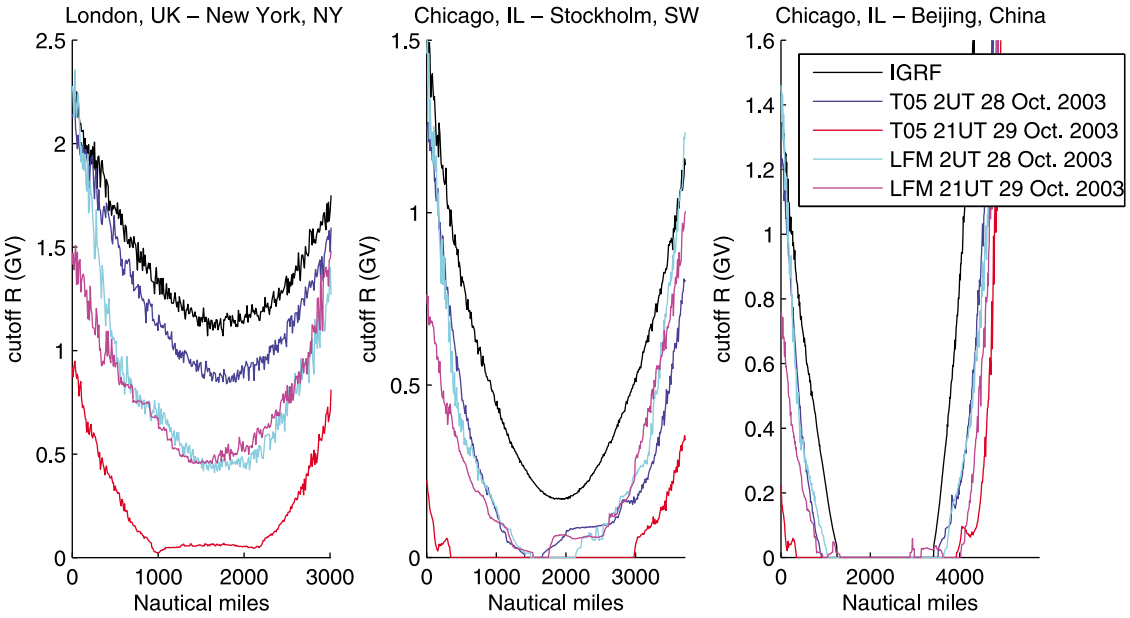

Figure 9. Cutoff rigidities along three flight routes computed in three different field models: IGRF, TS05, and MHD. The TS05 and MHD cutoffs were computed with flights starting during a prestorm quiet period at 0200 UT on 28 October 2003 (blue and cyan curves) and starting during the main phase of the storm at 2100 UT on 29 October 2003 (red and magenta curves).

atmosphere above the flight route in the prestorm fields and nearly all SEPs are allowed access during the storm. This is seen by comparing the TS05 prestorm (blue curve) and storm time (red curve) cutoff rigidities shown in Figure 9. Since the interplanetary SEP flux is undiminished by magnetic shielding above the open/closed boundary, the Chicago to Beijing flight has zero cutoff rigidity over most of its flight route regardless of geomagnetic conditions and does not experience as great a difference between prestorm and storm time SEP exposure.

[36] There is little difference between the prestorm and storm time cutoff rigidities computed in the LFM MHD fields indicated by the cyan and magenta curves, except during the early portion of the flights between ~0 and 500 nautical miles when there is a strongly southward IMF B_Z of ~–20 nT at ~2100–2200 UT on 29 October 2003 (shown in Figure 4). The LFM MHD prestorm and storm time cutoffs do not differ significantly over the later portion of the flights since the ring current, which is the primary source of the cutoff suppression during this period, is not well modeled by an MHD description of the magnetosphere. The coupled LFM-RCM model, which is not yet fully operational, is expected to improve the accuracy of CISM's physics-based geomagnetic field model in the inner magnetosphere.

[37] The operational NAIRAS model will utilize cutoff rigidities interpolated from a global latitude-longitude grid. In the work presented here however, to determine the difference between prestorm and storm time dose and provide a baseline for future studies, cutoff rigidities are computed approximately every 10 nautical miles along the flight routes. No attempt has been made to optimize the cutoff rigidity calculation along the flight trajectory by computing cutoffs at a minimum number of latitude-longitude points. For example, cutoff rigidities along the London to New York flight are computed at ~300 locations, where clearly this resolution is not needed to obtain cutoff rigidities accurate to a few percent of R_C. The small variations in R_C along the flight paths seen in Figure 9 are due to numerical error and can be taken as an estimate of the numerical inaccuracy associated with the cutoff rigidity search algorithm. The resolution of the global latitude-longitude grid and flight trajectory grid points required in an operational space weather prediction model are yet to be determined.

4. Summary and Discussion

[38] During the 26–31 October 2003 solar-geomagnetic event the maximum suppression of the cutoff is ~1 GV, occurring during the main phase of the storm at ~2100 UT on 29 October 2003 in the midlatitudes on the duskside of the Earth. The maximum cutoff suppression is due mainly to an enhanced partial ring current which also causes a strong local time dependence in the cutoff suppression. The cutoff is also significantly lowered before the main phase of the storm by the arrival of an interplanetary shock at 0611 UT on 29 October 2003. The maximum suppression of the cutoff due to the shock is ~0.5 GV, about one half of the maximum suppression during the main phase of the storm, and occurs in the midlatitudes on the nightside. Surprisingly, the maximum suppression

of the cutoff occurs well before the Dst reaches a minimum, partly due to the influence of a strongly southward IMF B_Z. The maximum suppression of the cutoff during the storm occurs when the Dst is ~100 nT above its minimum value.

[39] It is also noteworthy that prior to the arrival of the shock the northern portion of the continental United States is between cutoff rigidity contours of 1 GV and 2 GV, while during the main phase of the storm most of the northern United States is between 0.1 GV and 1.0 GV contours. The rigidities 0.1, 1.0 and 2.0 are equivalent to proton energies of 5.3, 430, and 1300 MeV, respectively.

[40] At the midlatitudes to high latitudes, the uncertainty associated with the cutoff latitude determination is $\Delta\lambda$ = 1.8°. In addition to inaccuracies in the numerical model, the difference between modeled and observed values is also due to uncertainties in the cutoff observation. In some cases, the observed cutoff is not well defined due to spatial and temporal variations of the SEP flux in the polar cap region, e.g., as shown in Figure 5, also, as described by *Morfill and Quenby* [1971]. The uncertainty in the modeled cutoff latitudes is similar to that reported in previous studies; for example, *Kahler and Ling* [2002] compare cutoff latitudes modeled using the TS89 field model during nine geomagnetic storms and find on average that the modeled cutoff latitudes differ from observed by $\Delta\lambda$ = 2.5°. In agreement with the earlier study by Kahler and Ling, the modeled cutoff latitudes are found to be systematically poleward of the observed cutoff latitudes on average. We find that the mean difference between the absolute values of the modeled and observed cutoff latitudes (modeled minus observed) is 0.60°.

[41] In previous work, SEP and cosmic ray flux in the magnetosphere has been modeled using a look up table of vertical cutoff rigidities computed in T89 model geomagnetic fields, parametrized by location and the 3 h averaged Kp index [*Smart and Shea*, 2003; *Smart et al.*, 2006]. The two advancements in recent years that have made a real-time geomagnetic cutoff rigidity calculation a possibility are the development of accurate dynamic geomagnetic field models, that respond to changes in Dst, solar wind dynamic pressure and IMF, and an increase in computer power. The work presented here is not intended to address the computational requirements of a real-time cutoff computation using Lorentz trajectories. The CPU time used to compute the global maps shown in Figure 7 is ~12 h on a single 2.5 GHz processor; however, there are several planned modifications to the search algorithm that are expected to reduce this considerably. Also, the problem is trivially parallelized to as many processors as one would like, since no communication between the processors is necessary; that is, each processor can compute the rigidity at a subset of the required locations. A more detailed description of the cutoff rigidity search algorithm and complete assessment of the computational effort needed to obtain cutoff rigidities on a global grid or along a spacecraft trajectory will be included in future work.

[42] **Acknowledgments.** This material is based upon work supported by the National Aeronautics and Space Administration issued through the Applied Sciences Program and under grant NNX07AO77G issued through the LWS TR&T program. This material is also based upon work supported by the STC Program of the National Science Foundation under agreement ATM-0120950 Thank you to Chia-Lin Huang at Boston University and Larry Kepko at the University of New Hampshire for their help preparing the solar wind input file for the TS05 and LFM MHD geomagnetic field models. The authors are very grateful to their reviewers for assistance with this manuscript.

References

Baker, D. N., G. M. Mason, O. Figueroa, G. Colon, J. G. Watzin, and R. M. Aleman (1993), An overview of the Solar, Anomalous, and Magnetospheric Particle Explorer (SAMPEX) mission, *IEEE Trans. Geosci. Remote Sens.*, *31*(3), 531–541.

Bartlett, D. T. (2004), Radiation protection aspects of the cosmic radiation exposure of aircraft crew, *Radiat. Prot. Dosim.*, *109*(4), 349–355.

Belov, A., L. Baisultanova, E. Eroshenko, H. Mavromichalaki, V. Yanke, V. Pchelkin, C. Plainaki, and G. Mariatos (2005), Magnetospheric effects in cosmic rays during the unique magnetic storm on November 2003, *J. Geophys. Res.*, *110*, A09S20, doi:10.1029/2005JA011067.

Clilverd, M. A., C. J. Rodger, T. Ulich, A. Seppälä, E. Turunen, A Botman, and N. R. Thomson (2005), Modeling a large solar proton event in the southern polar atmosphere, *J. Geophys. Res.*, *110*, A09307, doi:10.1029/2004JA010922.

Dyer, C. S., F. Lei, S. N. Clucas, D. F. Smart, and M. A. Shea (2003), Calculations and observations of solar particle enhancements to the radiation environment at aircraft altitudes, *Adv. Space Res.*, *32*(1), 81–93.

Golightly, M. J., and M. Weyland (1997), Modeling exposures aboard the space shuttle from the August 1989 solar particle event, paper 13 presented at Impact of Solar Energetic Particle Events on Design of Human Missions, Cent. for Adv. Space Stud., Houston, Tex.

Jackman, C. H., M. T. DeLand, G. J. Labow, E. L. Fleming, D. K. Weisenstein, M. K. W. Ko, M. Sinnhuber, and J. M. Russell (2005), Neutral atmospheric influences of the solar proton events in October–November 2003, *J. Geophys. Res.*, *110*, A09S27, doi:10.1029/2004JA010888.

Kahler, S., and A. Ling (2002), Comparisons of high latitude E > 20 MeV proton geomagnetic cutoff observations with predictions of the SEPTR model, *Ann. Geophys.*, *20*(7), 997–1005.

Kress, B. T., M. K. Hudson, K. L. Perry, and P. L. Slocum (2004), Dynamic modeling of geomagnetic cutoff for the 23–24 November 2001 solar energetic particle event, *Geophys. Res. Lett.*, *31*, L04808, doi:10.1029/2003GL018599.

Labrador, A. W., R. A. Leske, S. Kanekal, B. Klecker, M. Looper, J. Mazur, and R. A. Mewaldt (2003), SAMPEX measurements of geomagnetic-cutoffs during the April 21, 2002 solar energetic particle event, paper presented at Storms 2 Workshop, Johns Hopkins Univ. Appl. Phys. Lab., Laurel, Md., Aug. 19–21.

Lee, D., and B. T. Kress (2008), Geomagnetic cutoff variations due to interplanetary shocks, *Eos Trans. AGU*, *89*(53), Fall Meet. Suppl., Abstract SM53A-1661.

Lemaitre, G., and M. S. Vallarta (1933), On Compton's latitude effect of cosmic radiation, *Phys. Rev.*, *43*(2), 87–91.

Leske, R. A., R. A. Mewaldt, E. C. Stone, and T. T. von Rosenvinge (2001), Observations of geomagnetic cutoff variations during solar energetic particle events and implications for the radiation environment at the space station, *J. Geophys. Res.*, *106*, 30,011–30,022, doi:10.1029/2000JA000212.

Lopez, R. E., S. Hernandez, M. Wiltberger, C.-L. Huang, E. L. Kepko, H. Spence, C. C. Goodrich, and J. G. Lyon (2007), Predicting magnetopause crossings at geosynchronous orbit during the Halloween storms, *Space Weather*, *5*, S01005, doi:10.1029/2006SW000222.

Lyon, J. G., J. A. Fedder, and C. M. Mobarry (2004), The Lyon-Fedder-Mobarry (LFM) global MHD magnetospheric simulation code, *J. Atmos. Sol. Terr. Phys.*, *66*(15–16), 1333–1350.

Mertens, C. J., B. T. Kress, M. Wiltberger, S. R. Blattnig, T. S. Slaba, S. C. Solomon, and M. Engle (2010), Geomagnetic influence on aircraft radiation exposure during a solar energetic particle event

in October 2003, *Space Weather*, *8*, S03006, doi:10.1029/2009SW000487.
Mewaldt, R. A., C. M. S. Cohen, A. W. Labrador, R. A. Leske, G. M. Mason, M. I. Desai, M. D. Looper, J. E. Mazur, R. S. Selesnick, and D. K. Haggerty (2005), Proton, helium, and electron spectra during the large solar particle events of October–November 2003, *J. Geophys. Res.*, *110*, A09S18, doi:10.1029/2005JA011038.
Morfill, G. E., and J. J. Quenby (1971), The entry of solar protons over the polar caps, *Planet. Space Sci.*, *19*, 1541–1577.
Orloff, S. M. (1999), A computational investigation of solar energetic particle trajectories in model magnetospheres, Ph.D. thesis, Rice Univ., Houston, Tex.
Press, W. H., B. P. Flannery, S. A. Teukolsky, and W. T. Vetterling (1992), *Numerical Recipes in C: The Art of Scientific Computing*, 2nd ed., Cambridge Univ. Press, Cambridge, U. K.
Shea, M. A., D. F. Smart, and K. G. McCracken (1965), A study of vertical cutoff rigidities using sixth degree simulations of the geomagnetic field, *J. Geophys. Res.*, *70*, 4117–4130.
Smart, D. F., and M. A. Shea (1994), Geomagnetic cutoffs: A review for space dosimetry applications, *Adv. Space Res.*, *14*(10), 787–797.
Smart, D. F., and M. A. Shea (2001), A comparison of the Tsyganenko model predicted and measured geomagnetic cutoff latitudes, *Adv. Space Res.*, *28*(12), 1733–1738.
Smart, D. F., and M. A. Shea (2003), The space-developed dynamic vertical cutoff rigidity model and its applicability to aircraft radiation dose, *Adv. Space Res.*, *32*(1), 103–108.
Smart, D. F., and M. A. Shea (2005), A review of geomagnetic cutoff rigidities for Earth-orbiting spacecraft, *Adv. Space Res.*, *36*(10), 2012–2020.
Smart, D. F., M. A. Shea, and E. O. Fluckiger (2000), Magnetospheric models and trajectory computations, *Space Sci. Rev.*, *93*(1–2), 305–333.
Smart, D. F., M. A. Shea, A. J. Tylka, and P. R. Boberg (2006), A geomagnetic cutoff rigidity interpolation tool: Accuracy verification and application to space weather, *Adv. Space Res.*, *37*(6), 1206–1217.
Störmer, C. (1955), *The Polar Aurora*, Oxford Univ. Press, London.
Swann, W. F. (1933), Application of Liouville's theorem to electron orbits in the Earth's magnetic field, *Phys. Rev.*, *44*(3), 224–227.
Toffoletto, F. R., S. Sazykin, R. W. Spiro, R. A. Wolf, and J. G. Lyon (2004), RCM meets LFM: Initial results of one-way coupling, *J. Atmos. Sol. Terr. Phys.*, *66*(15–16), 1361–1370.
Tsyganenko, N. A. (1989), A magnetospheric magnetic field model with a warped tail current sheet, *Planet. Space Sci.*, *37*, 5–20.
Tsyganenko, N. A. (1996), Effects of the solar wind conditions on the global magnetospheric configuration as deduced from data-based field models, in *Third International Conference on Substorms (ICS-3), Versailles, France, 12–17 May 1996*, edited by E. J. Rolfe and B. Kaldeich, *Eur. Space Agency Spec. Publ.*, *ESA SP-389*, 181–185.
Tsyganenko, N. A., and M. I. Sitnov (2005), Modeling the dynamics of the inner magnetosphere during strong geomagnetic storms, *J. Geophys. Res.*, *110*, A03208, doi:10.1029/2004JA010798.
Tylka, A. J., W. F. William, P. R. Dietrich, E. C. Boberg, C. Edward, J. H. Smith, and J. H. Adams (1996), Single event upsets caused by solar energetic heavy ions, *IEEE Trans. Nucl. Sci.*, *43*(6), 2758–2766.
Wang, W., M. Wiltberger, A. G. Burns, S. C. Solomon, T. L. Killeen, N. Maruyama, and J. G. Lyon (2004), Initial results from the coupled magnetosphere-ionosphere-thermosphere model: Thermosphere-ionosphere responses, *J. Atmos. Sol. Terr. Phys.*, *66*(15–16), 1425–1441.
Weygand, J. M., and J. Raeder (2005), Cosmic ray cutoff prediction using magnetic field from global magnetosphere MHD simulations, *Ann. Geophys.*, *23*(4), 1441–1453.

B. T. Kress, Department of Physics and Astronomy, Dartmouth College, HB6127 Wilder Laboratory, Hanover, NH 03755, USA. (bkress@dartmouth.edu)
C. J. Mertens, NASA Langley Research Center, Hampton, VA 23681-2199, USA.
M. Wiltberger, National Center for Atmospheric Research, High Altitude Observatory, Boulder, CO 80307, USA.